Received: 21 August 2020 | Revised: 10 February 2021 | Accepted: 21 February 2021

DOI: 10.1111/jace.17786

Journal of the American Ceramic Society

ORIGINAL ARTICLE

Flash sintering produces eutectic microstructures in Al_2O_3–$LaPO_4$ versus conventional microstructures in 8YSZ–$LaPO_4$

Yingjie Yang | **Daniel R. Mumm** | **Martha L. Mecartney**

Department of Material Science and Engineering, University of California, Irvine, CA, USA

Correspondence
Yingjie Yang, Department of Material Science and Engineering, University of California, Irvine, CA, USA.
Email: yingjiey@uci.edu

Funding information
National Science Foundation, Grant/Award Number: CMMI MEP 1662791

Abstract

While monazite ($LaPO_4$) does not flash sinter even at high fields of 1130 V/cm and temperatures of 1450°C, composite systems of 8YSZ–$LaPO_4$ and Al_2O_3–$LaPO_4$ have been found to more readily flash sinter. 8YSZ added to $LaPO_4$ greatly lowered the furnace temperature for flash to 1100°C using a field of only 250 V/cm. In these experiments, α-Al_2O_3 alone also did not flash sinter at 1450°C even with high fields of 1130 V/cm, but composites of Al_2O_3–$LaPO_4$ powders flash sintered at 900-1080 V/cm at 1450°C. Alumina–monazite (Al_2O_3–$LaPO_4$) composites with compositions ranging from 25 vol% to 75 vol% Al_2O_3 were flash sintered with current limits from 2 to 25 mA/mm^2. Microstructures were evaluated by scanning electron microscopy (SEM) and transmission electron microscopy (TEM). A eutectic microstructure was observed to form in all flash sintered Al_2O_3–$LaPO_4$ composites. With higher power (higher current limits), eutectic structures with regular lamellar regions were found to coexist in the channeled region (where both the current and the temperature were the highest) with large hexagonal-shaped α-Al_2O_3 grains (up to 75 μm) and large irregular $LaPO_4$ grains. With lower power (lower current limits), an irregular eutectic microstructure was dominant, and there was minimal abnormal grain growth. These results indicate that Al_2O_3–$LaPO_4$ is a eutectic-forming system and the eutectic temperature was reached locally during flash sintering in regions. These eutectic microstructures with lamellar dimensions on the scale of 100 nm offer potential for improved mechanical properties.

KEYWORDS

alumina, composites, field assisted sintering technology, monazite, yttria-stabilized zirconia

1 | INTRODUCTION

Flash sintering is a novel manufacturing technique that applies an electrical field across a ceramic green body, while heating it in a furnace.[1-3] As the material sinters, the current induces joule heating, which assists in fast densification or enhanced reaction mixing. Over the past decade, flash sintering has shown promise in reducing sintering costs, increasing densification efficiency, promoting reaction sintering, etc.[4] In the current era of energy conservation to preserve the environment, it is important to find a way to reduce energy consumption for material processing.[5,6] Due to its nature of fast transformation and densification, flash sintering can induce non-equilibrium transitions and lead to unconventional microstructures which may have interesting thermal and mechanical properties.[1,7,8]

The prerequisite conditions and phenomena of flash sintering are material specific.[1,9,10] 8 mol% Y_2O_3-stabilized ZrO_2 (8YSZ) has been well established to flash sinter easily at low temperatures and low voltages.[1,11] The presence of 8YSZ can assist flash sintering for other materials in a

composite.[12-15] Some single phase ceramics such as alumina are difficult to flash sinter,[16] but can flash easier when a constituent of a composite or through reaction sintering.[17-19] For example, Kok et al[12] observed densification in 3 seconds at 250 V/cm and furnace temperature 1250°C with a composite of α-Al_2O_3, $MgAl_2O_4$ spinel, and cubic 8YSZ, while in contrast, flash sintering of single phase Al_2O_3 or single phase spinel requires much higher voltage and higher furnace temperature to reach similar density.[20,21] The applied electric field during flash sintering generates a current that heats the sample far above the furnace temperature but other phenomena may also be involved, including enhanced flash sintering by the presence of heterointerfaces.[22]

Research on flash sintering of binary structural ceramic composite systems which contain heterointerfaces is limited[19,23-26] and will be addressed in this paper. The specific systems studied include monazite $LaPO_4$, 8YSZ, and Al_2O_3 as single phases and as composites. All of these ceramics require high temperatures and long times to sinter conventionally. $LaPO_4$ has several major applications. It may be utilized as an interphase coating in ceramic fiber-matrix composites providing low-toughness interfaces, which can greatly enhance the damage tolerant behavior.[27,28] Morgan et al[29] found that the addition of interphase $LaPO_4$ to an Al_2O_3 matrix reinforced with sapphire fibers greatly improved the fracture resistance due to reduced crack propagation through the fibers, by crack deflection and debonding along the weak $LaPO_4/Al_2O_3$ interface. Similar effects were observed in multilayered ZrO_2–$LaPO_4$ composites, and persisted up to 1600°C,[27] and also in YSZ–$LaPO_4$ to 1000°C.[30,31] The Al_2O_3–$LaPO_4$ composite system has great promise as a high temperature structural ceramic material.[32,33] ZrO_2–$LaPO_4$ has been proposed for thermal barrier coating applications.[34] Composites with at least 30 wt% $LaPO_4$ in Al_2O_3 and at least 25% $LaPO_4$ in ZrO_2 enable them to be machined by WC tooling due to the weak interfaces as monazite does not bond well to oxide ceramics.[35-37]

2 | EXPERIMENTAL

2.1 | Materials

The following raw materials were used to fabricate the samples: α-Al_2O_3 powders (99.99%, Taimei TM-DAR, Japan), 8 mol% Y_2O_3 stabilized cubic ZrO_2 powders (TZ-8YS, Tosoh, USA) and hydrated $LaPO_4$ rhabdophane powders ($LaPO_4 \cdot xH_2O$, Strem Chemicals, USA). The hydrated $LaPO_4$ powders were annealed at 1000°C for 1 hour to ensure removal of any hydrate and generate the monazite phase of $LaPO_4$.

Composites of alumina and monazite were prepared by mixing in certain volume percentages (25%, 50%, 75%) alumina with the monazite powders, prepared by attrition milling (HD-01, Union Process, USA) for 8 hours in isopropyl alcohol to ensure a homogeneous mixture. Similarly, composites of 8YSZ and monazite were prepared with 25 vol% and 50 vol% 8YSZ. Media used for milling was 0.5-mm high-wear-resistant zirconia grinding media (YTZ Grinding Media, Tosoh, USA) for composites containing 8YSZ, or 0.5-mm alumina grinding media (99.5%, Union Process, USA) for composites containing Al_2O_3. Mixtures were dried with a rotary evaporator, then combined with 2.5 wt% of polyvinyl alcohol (PVA) dissolved in water. These slurries were dried again at 80°C, products ground with a mortar and pestle, and sieved to below 106 μm.

To prepare green bodies for flash sintering, powders were pressed in a dog-bone shaped mold in a uniaxial press (Carver, USA) at 260 MPa for 5 minutes. After PVA binder burnt out in an ashing furnace at 600°C for 1 hour, the relative green body density was 50 ± 2%. Dog-bone samples were made with a hole at each end with a gauge length of 13.5 mm, and a cross section of approximately 3.5 × 1.6 mm.

2.2 | Sintering

Flash sintering experiments were carried out with resistance furnace heat and an electrical field applied to the sample at the same time. For comparison, some samples were conventionally sintered at 1500°C for 5 hours. As shown in Figure 1, samples were placed in a horizontal tube furnace (ATS, USA), with a pair of Pt hooks that connect the holes at the ends of the dog-bone samples with the resistance wires (Kanthal, Sweden) that lead to the power supply (Glassman High Voltage, USA) outside of the furnace controlled by a computer. Platinum paste was applied around the connection to ensure good conduction. The computer also records the voltage and current measured by a multimeter (Newark, USA), and records videos

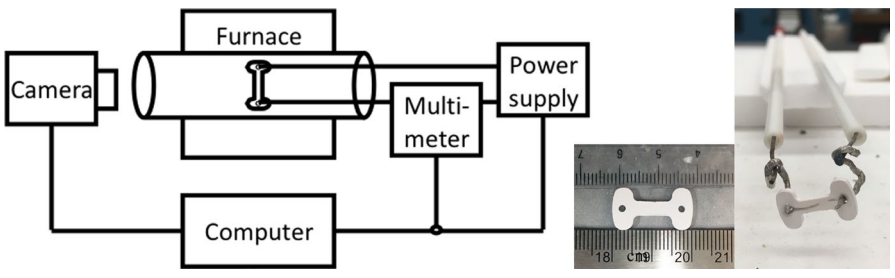

FIGURE 1 Sketch of experimental setup for flash sintering, photographs of a green dog-bone sample and a flashed dog-bone sample with electrodes attached [Color figure can be viewed at wileyonlinelibrary.com]

of the flash sintering experiments taken by a CCD camera (The Imaging Source, USA).

The onset of the flash phenomenon is controlled by the furnace temperature and the applied voltage. The flash of the sample is marked with a sudden spike in the measured current, when the power supply then automatically switches to current control when the preset current limit was reached. The current limit was set to avoid power overshoot and to tailor the microstructure of the sample as the current multiplied by the voltage equals the power input into the sample. Voltage applied on the sample was determined by the potential drop over the initial length between the two electrical contacts. The current density limit applied on the sample was calculated by the current divided by the initial cross-sectional area of the gauge section.

The flash sintering experiments were conducted by first heating with constant voltage applied, then voltage increase with constant temperature (if needed), and a hold of the flash under current control. At the start of the experiment, an electrical field with a constant voltage density of 250 V/cm was applied to the sample in the furnace. The furnace temperature was ramped up from room temperature to 1450°C or until flash occurs. If flash occurred at a furnace temperature below 1450°C, it was held for 8-30 seconds, then both the power supply and the furnace were turned off, as shown in Figure 2A. If flash did not occur with 250 V/cm when the temperature reached 1450°C, this condition was held for 5 min to stabilize the temperature throughout the sample and then the voltage was increased with increments of 100 V/cm every 2 minutes to a maximum of 1130 V/cm, as shown in Figure 2B. If the sample flashed below the maximum capacity of the power supply was reached (1130 V/cm), this condition at the flash onset was held for 5.5-10 seconds before the furnace and power supply were shut off. In all cases, the samples were cooled in the furnace to room temperature after the power was turned off.

2.3 | Characterization

The phase composition, elemental composition, and microstructure of the flash sintered samples were characterized. X-ray diffraction (Rigaku SmartLab, Japan) was used to confirm complete phase transformation from hydrate $LaPO_4$ to monazite, verify the purity of alumina and 8YSZ, and the compositions of the composites after mixing. The analysis was also done on the dog-bone samples after flash sintering. Scanning electron microscopy (SEM, FEI Magellan XHR, USA) was used to image the sample surface with both secondary and backscatter electrons, after sputter coating it with iridium (Q150T, EMS, USA). Energy dispersive x-ray spectroscopy (EDS) (Oxford Instruments, United Kingdom) was conducted on samples coated with carbon (EM ACE200, Leica, Germany). Electron backscatter diffraction (EBSD) (Tescan GAIA3 SEM-FIB, Czech Republic) and transmission Kikuchi diffraction (TKD) (FEI Quanta 3D FEG, USA) was used to analyze crystallographic orientations. Transmission electron microscopy imaging and diffraction (Philips CM-20, USA) were used to investigate crystalline microstructure with samples prepared by focused ion beam system (FIB) (Tescan GAIA3 SEM-FIB, Czech Republic; FEI Quanta 3D FEG, USA).

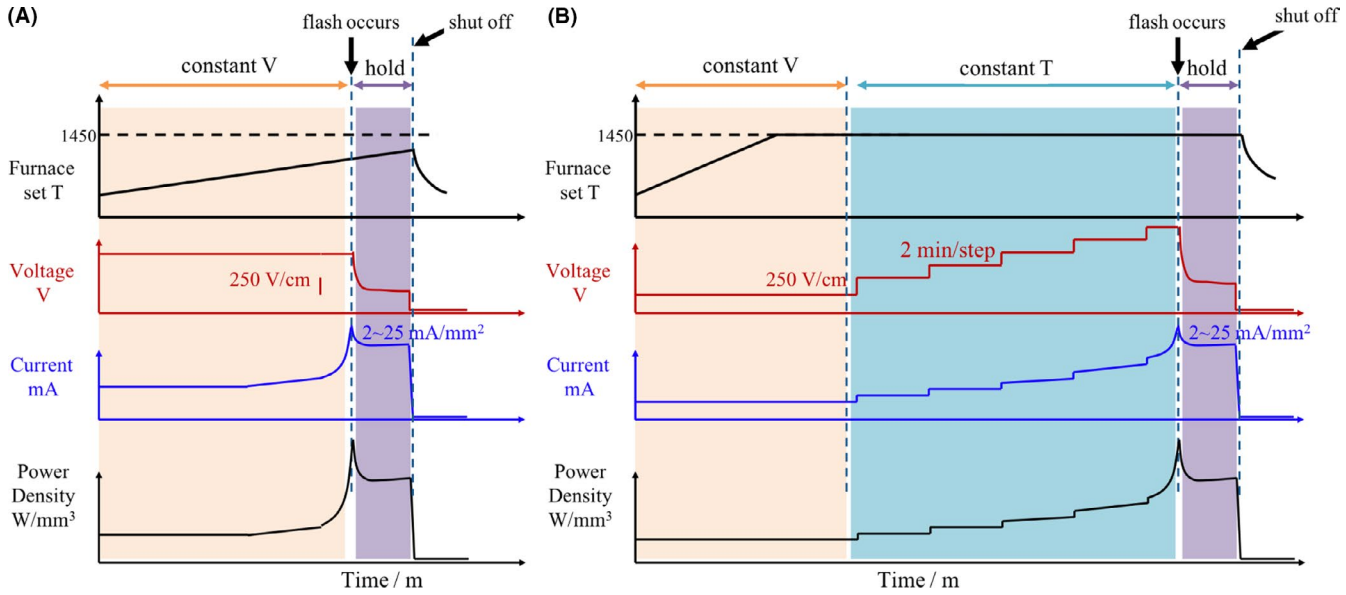

FIGURE 2 Two types of flash sintering conditions: (A) constant 250 V/cm is applied and the temperature is ramped up to 1450°C or the temperature that flash occurs and (B) temperature ramp to 1450°C with 250 V/cm then the voltage is increased by steps until flash occurs [Color figure can be viewed at wileyonlinelibrary.com]

3 | RESULTS

3.1 | The onset condition for flash is dependent on composition

The flash conditions are summarized in Table 1 for the different compositions, average onset voltages (ranging from 250 V/cm to 1130 V/cm), current limits (2 mA/mm^2 to 25 mA/mm^2), furnace temperatures at onset of flash (780°C to 1450°C), estimated sample temperatures from joule heating, and general features of the resultant microstructures.

Pure 8YSZ samples and composite samples containing 8YSZ all flashed at temperatures below 1450°C with a constant applied voltage of 250 V/cm. The onset temperature of flash increased when the concentration of 8YSZ decreased (see Table 1). Pure 8YSZ samples flashed at an average temperature of 780°C; when 50% 8YSZ–50% $LaPO_4$ composites were tested, the samples flashed at around 1110°C. Dropping the amount of 8YSZ from 50 vol% to 25 vol% required a higher furnace temperature of 1379°C.

In this study, single-phase monazite $LaPO_4$ or Al_2O_3 samples were not able to flash at 1450°C, even with applied voltages as high as the maximum capability of the power supply (1130 V/cm). However, samples of Al_2O_3–$LaPO_4$ composites were able to flash at lower voltages even at the same maximum furnace temperature of 1450°C. For samples containing 50% Al_2O_3-50% $LaPO_4$, the average onset voltage was 1080 V/cm. The average onset voltages for samples with other compositions were noticeably lower, 980 V/cm for samples with 25% Al_2O_3 and 935 V/cm for 75% Al_2O_3.

During the flash, the gauge sections of the dog-bone samples started to visibly brighten coinciding with the current spike, providing visualization of the flash region. Flash phenomena in all samples started with a nearly straight pathway that connected the two electrodes, shown in Figure 3. In all samples containing 8YSZ, the flash quickly propagated across the gauge section to form a continuous brightness with a gradient to the lateral edges. In samples containing Al_2O_3 and monazite, in contrast, the bright flash regions had abrupt boundaries and regions where the current was concentrated and channeled. The sharp boundaries of flash in those samples correlate with an abrupt change in the final microstructure across the gauge section, as will be shown later. In some cases, the channeling traveled from the front to the back through the thickness of the sample and connected the two electrodes on the opposite surfaces, as shown in Figure 3C.

3.2 | Microstructure depends on the flash condition and composition

No new phases were formed, comparing XRD of the original powder mixtures to flash sintered samples.

For 8YSZ–$LaPO_4$ composites, flash sintered samples show polycrystalline morphology similar to conventionally sintered samples. The flash sintered dog-bone samples show equiaxed grains across the gauge section without significant channeling or boundaries, with slightly larger grains at the center and slightly smaller grains on the lateral edges of the gauge section, as shown in Figure 4. This agrees with the flash phenomenon shown in Figure 3, as the brightness where the current would be highest is higher at the center, lower at the gauge section lateral edges, and continuous across the gauge section. Under the imaging conditions utilized, the backscattering coefficients for 8YSZ and monazite are similar, such that negligible backscatter electron (BSE) imaging contrast exists between the two phases and no visual differentiation of the two can be directly observed.

Flash sintered samples of Al_2O_3–$LaPO_4$ composites, in contrast, show drastically different morphologies compared to the 8YSZ–$LaPO_4$ composites. At the lateral edges, the microstructure consists of randomly oriented polycrystalline grains of both phases. A grooved region in the center can be observed macroscopically with abrupt boundaries on the sample surface, corresponding to the distinct brightened region during the flash shown in Figure 3. In the channeled regions, there is virtually no equiaxed polycrystalline microstructure for Al_2O_3–$LaPO_4$ composites. Instead, the channeled regions contain eutectic microstructures, highly faceted large grains, and grains with abnormal grain growth. Figure 5 illustrates the general regions where the corresponding microstructures are found.

The contrast difference for Al_2O_3 ($\rho = 4$ g/cm^3) and $LaPO_4$ ($\rho = 5$ g/cm^3) in BSE imaging clearly reveals each phase (Figure 6) on the surface of the sample. Images in Figure 6 are taken from the channeled regions as indicated in Figure 5. In this case, the backscattering coefficients of these two phases are quite distinct, and readily facilitate contrast differentiation. Alumina grains show a darker contrast because of the lower Z contrast while monazite grains show lighter contrast under the current backscatter imaging conditions. Eutectic structures show an intermediate grey contrast at low magnification due to the intertwined morphology of finely layered eutectic. Polycrystalline regions at the lateral edges show a clear mixture of randomly arranged bright and dark grains (polycrystalline structure in Figure 6).

Distinct boundaries can be seen on the surface of Al_2O_3–$LaPO_4$ composites, marked by the contrast change that represent the abrupt change of microstructure from eutectic to polycrystalline (dotted lines in Figure 6). The center region that shows eutectic microstructure corresponds to the channeled region shown in Figure 3. Highly faceted alumina grains and monazite grains with abnormal grain growth appear in the center region on the surface, embedded in the eutectic structure, when a high current density is applied. Figure 6A clearly shows hexagonal

TABLE 1 Compositions, parameters, and microstructures of the flash-affected regions (estimated sample temperatures are calculated with the black-body radiation (BBR) model in Equation 1 using emissivity values of 1 and 0.4 as explained in Discussion)

Composition (vol %)	Flash?	Mean E-field (V/cm) ±SD	Current limit (mA /mm^2)	Mean maximum $T_{furnace}$ (°C)	BBR $T_{estimated}$ (°C)	Flash hold time (s)	Microstructural features
8YSZ	Yes	250	25	777 ± 9	1390-1670	10	Enhanced sintering
50%–50% 8YSZ–$LaPO_4$	Yes	250	25	1110	1510-1750	9-30	Enhanced sintering, uniform grains of both phases, minor cracking
25%–75% 8YSZ–$LaPO_4$	Yes	250	25	1393 ± 24	1670-1860	10	Enhanced sintering, uniform grain size, minor cracking
Al_2O_3	No	1130	25	1450	N/A	N/A	No significant enhanced sintering
$LaPO_4$	No	1130	25	1450	N/A	N/A	No significant sintering
25%–75% Al_2O_3-$LaPO_4$	Yes	990 ± 42	25	1450	2150-2510	8	Eutectic (regular), equiaxed $LaPO_4$ grains
50%–50% Al_2O_3-$LaPO_4$	Yes	1080 ± 53	25	1450	2190-2570	8	Eutectic (regular & irregular), bigger hexagonal Al_2O_3, $LaPO_4$ grain growth
	Yes		15	1450	1970-2270	6	Eutectic (regular & irregular), hexagonal Al_2O_3, $LaPO_4$ grain growth
	Yes		5	1450	1680-1840	8	Eutectic (regular & irregular), smaller hexagonal Al_2O_3, $LaPO_4$ grain growth
	Yes		2	1450	1560-1650	10	Eutectic (mostly irregular)
75%–25% Al_2O_3-$LaPO_4$	Yes	900 ± 71	5	1450	1640-1800	8	Eutectic (no long-term order), equiaxed Al_2O_3 grains

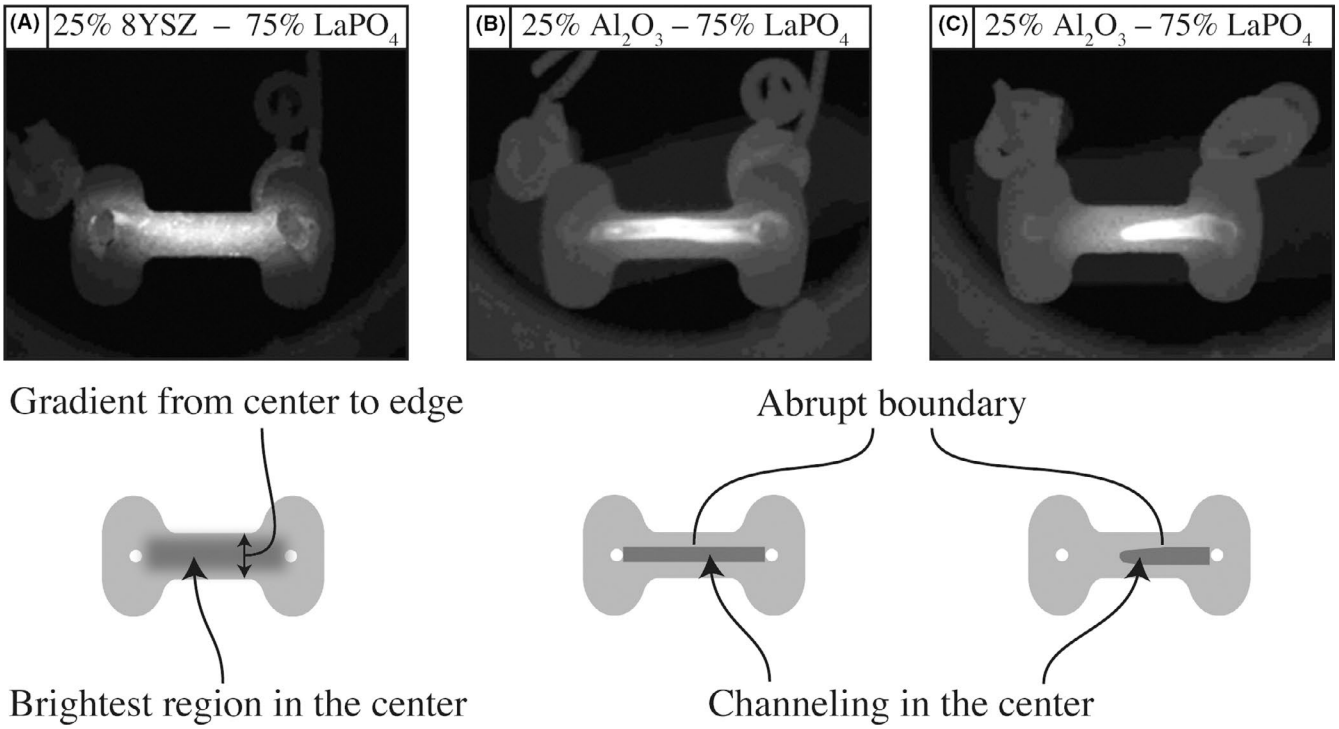

FIGURE 3 Photos of samples during flash and sketches of the flash region

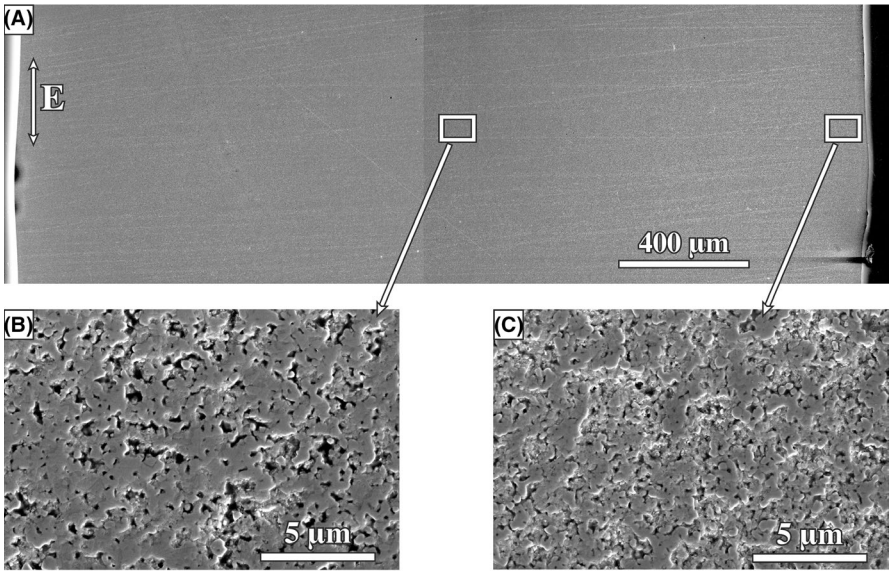

FIGURE 4 SEM images of the polished top surface in a 50-50 vol% 8YSZ–$LaPO_4$ sample (250 V/cm, 25 mA/mm^2, 30 s, 1110°C) showing (A) uniform structure across the gauge section at low magnification, (B) polycrystalline grains in the center region and (C) polycrystalline grains on the lateral edge. (The sample did not fully densify due to the short time and low temperature but the images demonstrate a fairly uniform structure with some slight differences in grain size and pore size from the center to the lateral edge.)

and elongated faceted Al_2O_3 grains on the surface in the centermost region of the gauge section, as well as large irregular monazite grains, found on the surface of a 50% Al_2O_3-50% $LaPO_4$ sample. Adjacent to the centermost region is a grey contrast that represents the eutectic structure, which will be shown in detail later. On the edge of samples for all three compositions, a polycrystalline microstructure was observed that was similar to conventionally sintered Al_2O_3–$LaPO_4$. Large cracks from thermal shock can be seen throughout the sample as the flash sintering parameters and the cooling rate were not optimized.

3.3 | Eutectic microstructures

Eutectic microstructures are represented by a gray contrast at low magnification. When observed closely, two types of eutectic structures coexist due to varying thermal profiles that can exist during flash sintering, and they form domains in the channeled regions. Figure 7A shows regular lamellar eutectic structures that are parallel layers of alternating Al_2O_3 and $LaPO_4$ grains. The monazite grains can spherodize in the alumina matrix and form a dashed line. A different type of

eutectic microstructure, the "irregular" eutectic structure (also characterized as anomalous[38,39]) that shows randomized orientation and no long-term order, exists on the sample surface as well, as shown in Figure 7B. These two morphologies can form domains and coexist in the channeled region, as shown later.

When the flashed composition is not 50-50% Al_2O_3–$LaPO_4$, the eutectic structure is found to exist in areas between grains of the dominant phase, as presented in Figure 8. In samples with Al_2O_3 content reduced to 25%, the center region of the gauge section is dominated by a brighter $LaPO_4$ phase, the rounded grains are surrounded by eutectic microstructures, as shown in Figure 8A. When Al_2O_3 content was increased to 75%, the center region of the image was dominated by darker faceted Al_2O_3 grains, with eutectic structures at the grain boundaries, as shown in Figure 8B.

Colonies formed by the eutectic can be observed from the cross section of the samples, as shown in Figure 9. The region

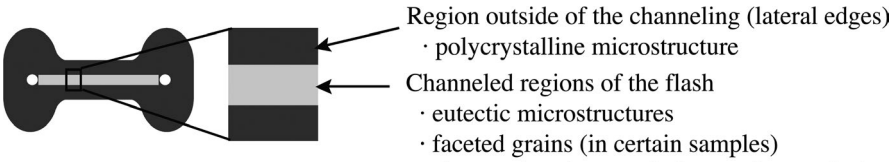

FIGURE 5 Sketch of a dog-bone sample and the locations of different structures that exist across the gauge section

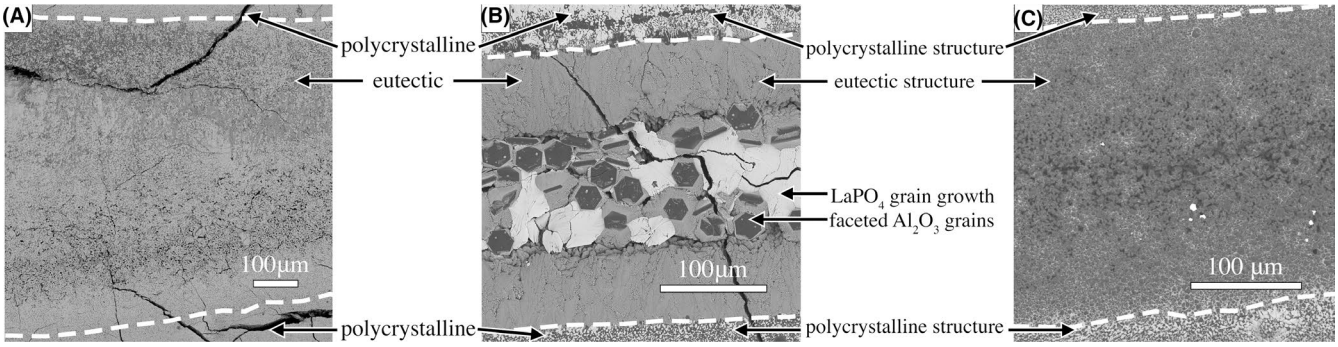

FIGURE 6 Channeled regions (bounded by lines) are similar on the surfaces in flash sintered Al_2O_3/$LaPO_4$ samples made under the same current limits (5 mA/mm^2) but with different alumina content: (A) 25-75% Al_2O_3-$LaPO_4$ (1000 V/cm 8 s) (B) 50-50% Al_2O_3-$LaPO_4$ (1050 V/cm 8 s) showing hexagonal alumina grains and large irregular shapes of monazite (C) 75-25% Al_2O_3-$LaPO_4$ (850 V/cm 8 s) flashed at a comparatively lower voltage

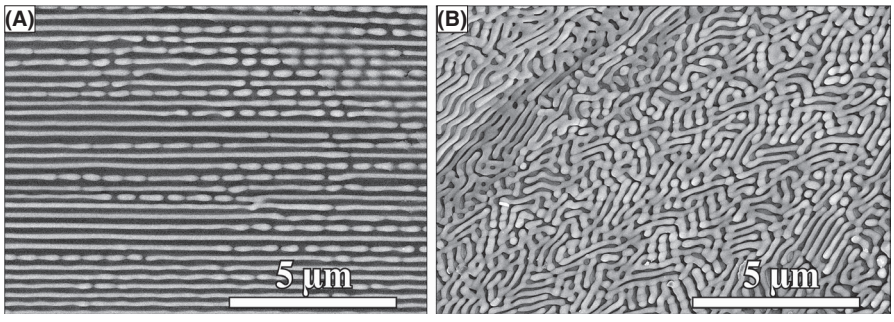

FIGURE 7 BSE images of the different eutectic microstructures on the surface of a 50-50% Al_2O_3-$LaPO_4$ sample (1100 V/cm, 25 mA/mm^2, 8 s) (A) regular lamellar eutectic-like structure (B) irregular eutectic-like structure: dark grains are alumina, bright grains are monazite

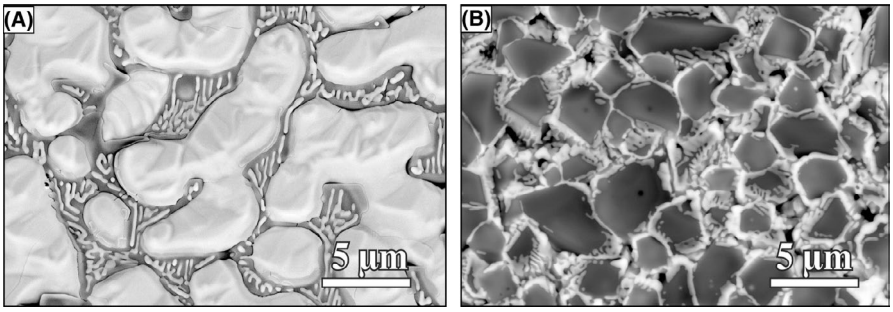

FIGURE 8 BSE images of the eutectic microstructures between grains of the dominant phase on the surface of (A) 25-75% Al_2O_3-$LaPO_4$ (1050 V/cm, 25 mA/mm^2, 8 s) (B) 75-25% Al_2O_3-$LaPO_4$ (950 V/cm, 5 mA/mm^2, 8 s)

with eutectic microstructure is within a roughly semicircle shape on the cross section, indicating that the flash channeled region was concentrated in a semi-cylindrical shaped volume along the gauge section. (The flash channeled region sometimes connects from the top to the bottom of the sample from one end to the other.) The borders of the colonies seen in the interior are marked by coarser alumina and monazite grains.

3.4 | Hexagonal alumina grains

The other type of unique microstructural feature present in the flashed region of the Al_2O_3–$LaPO_4$ composites is highly faceted alumina grains observed on the surface. Many alumina grains have a hexagonal shape close to a geometrically regular hexagon that is both equilateral and equiangular. Other large alumina grains have an elongated hexagonal shape that is close to equiangular. The faceted alumina grains, the thicknesses of which are estimated to range between 0.5 and 3 μm, are on the surface of a matrix of eutectic structures and monazite grains.

Figure 10A,B shows the surface of 50%-50% Al_2O_3–$LaPO_4$ samples made with current limits 25 mA/mm^2, (C) and (D) shows a sample made with 5 mA/mm^2, respectively. Comparing the grain sizes of Figure 10A,B or C,D, the size of the hexagonal grains is much smaller when the current limit is reduced from 25 to 5 mA/mm^2. The diameters of the regular hexagonal single crystals of alumina reach 75 μm when the sample is flash sintered by 25 mA/mm^2, but only half that size with 5 mA/mm^2. When the current limit was set to 2 mA/mm^2, no faceted alumina grains or large monazite grains was observed.

The equiangular appearance of the Al_2O_3 crystals can be attributed to the crystalline orientations of the hexagonal grains. Figure 11A shows the TEM sample made from milling perpendicular to one of the edges of a hexagonal alumina grain. The alumina large crystals are surrounded by a eutectic microstructure. TEM diffraction confirms that the surface of the hexagonal-shaped grains is normal to [0 0 0 1], so it is the basal plane of the pseudo-hexagonal lattice. The grain edges are normal to <1 1 $\bar{2}$ 0>. EBSD scans confirmed the same orientation throughout a hexagonal grain on the surface indicating it is a single crystal of sapphire (Figure 11B). This grain was located on the side of the center groove and appears slanted because tilting in the SEM was limited by the EBSD configuration. It is worth noting that transmission Kikuchi diffraction results show that the Al_2O_3 grains in the eutectic microstructures near the single-crystal Al_2O_3 have similar orientations as the faceted grain.

The other commonly observed microstructural feature is that the hexagonal alumina crystals can be seen as a collection of six triangles with monazite on the surface of half of them (Figure 10). The regions with monazite correspond to rough surfaces with a lower EBSD signal as well (Figure 11). FIB sectioning showed no existence of monazite inside the hexagonal alumina grains.

3.5 | Increased current limit increases power density and affects microstructure

The onset temperature and voltage required for flash vary depending on sample composition but did not greatly affect the microstructure of the flash sintered samples. However, the current limit of flash sintering has a significant influence on the width of the channeled region and the microstructure

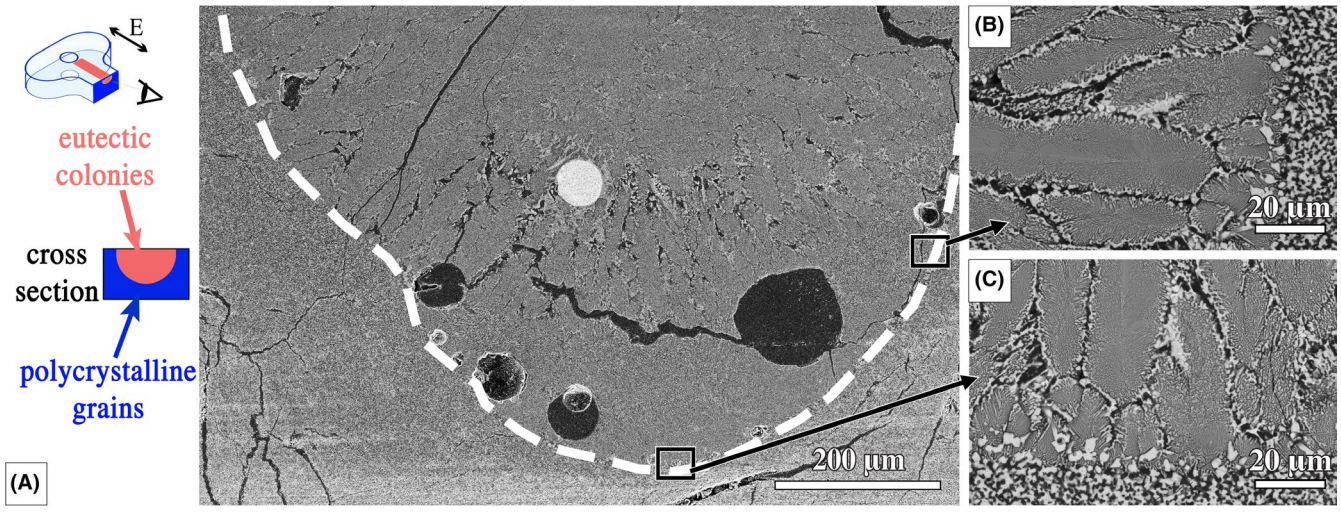

FIGURE 9 BSE images of a polished cross-section of a flash-sintered 50-50% Al_2O_3-$LaPO_4$ sample (25 mA/mm^2, 950 V/cm, 18 s) that (A) shows channeling does not span the entire sample thickness. (B) and (C) show the interior region that has eutectic colonies which appear to solidify normal to the polycrystalline regions of the randomly oriented alumina and monazite grain which did not melt. (The bright circular region in the center is a drop of Pt, black circular regions are pores filled with epoxy.) [Color figure can be viewed at wileyonlinelibrary.com]

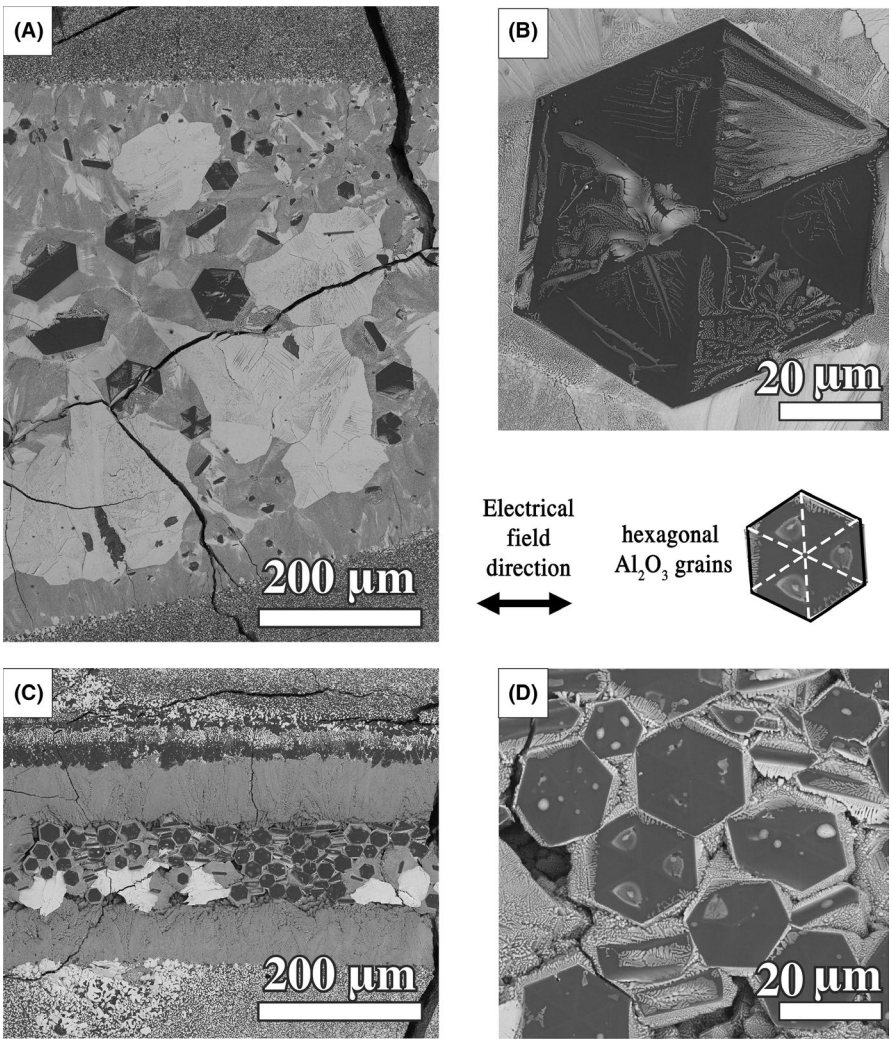

FIGURE 10 BSE images of the different grain sizes existing on the surface obtained by flash sintering 50-50% Al_2O_3-$LaPO_4$ with changing the current; (A) and (B) processed with a current limit of 25 mA/mm^2 (950 V/cm, 5.5 s), (C) and (D) processed with a current limit of 5 mA/mm^2 (1050 V/cm, 8 s). A higher current density, which results in higher power, creates larger grains of both hexagonal alumina and monazite

of the samples. Figure 6 shows two samples of different compositions flash sintered with the same current limit. The sizes of the center flash sintered region are nearly the same, indicating similar thermal profiles across the gauge section.

When samples with the same composition are flashed with different current limits, it is clear that the width of the channeled region that corresponds to flash increases with a higher applied current. Figure 12 shows the low-magnification images of 50-50% Al_2O_3–$LaPO_4$ samples flash sintered with maximum current limits of 25 mA/mm^2, 5 mA/mm^2, and 2 mA/mm^2. All samples have polycrystalline microstructure on the outside of the gauge section and eutectic microstructure at the center. The width of the channeled region that was subjected to melting and resolidification is the largest (920 μm) when the sample was flashed with the highest current limit 25 mA/mm^2, but only 260 μm when flash sintered with 5 mA/mm^2, and then even lower at 100 μm with 2 mA/mm^2. It has also been found that when the current limit is constant, but the increasing flash hold time was increased, the width of the channeled region increases as well.

Changing the current limit also changes the morphology of the microstructure. A low current limit of 2 mA/mm^2 does not produce large hexagonal alumina grains or abnormally large monazite grains with abnormal grain growth but creates only the eutectic microstructure (Figure 12C), in contrast with samples flash sintered with a higher enough current limit ($\geq$ 5 mA/mm^2 in this study).

Moreover the morphologies of the eutectic microstructure can be tailored by changing the current limit of the flash. Both regular lamellar and irregular eutectic structures appear in samples processed with higher currents (Figure 13A). When the current limit is reduced to 5 mA/mm^2, irregular eutectic structure is the primary morphology throughout the channeled region (Figure 13B), more typical of coupled growth with the lower current.

4 | DISCUSSION

4.1 | What promotes flash?

The onset conditions for flash sintering are different for the different compositions, as would be expected.[40] All 50%-50% Al_2O_3–$LaPO_4$ composites flashed within ±50 V. When

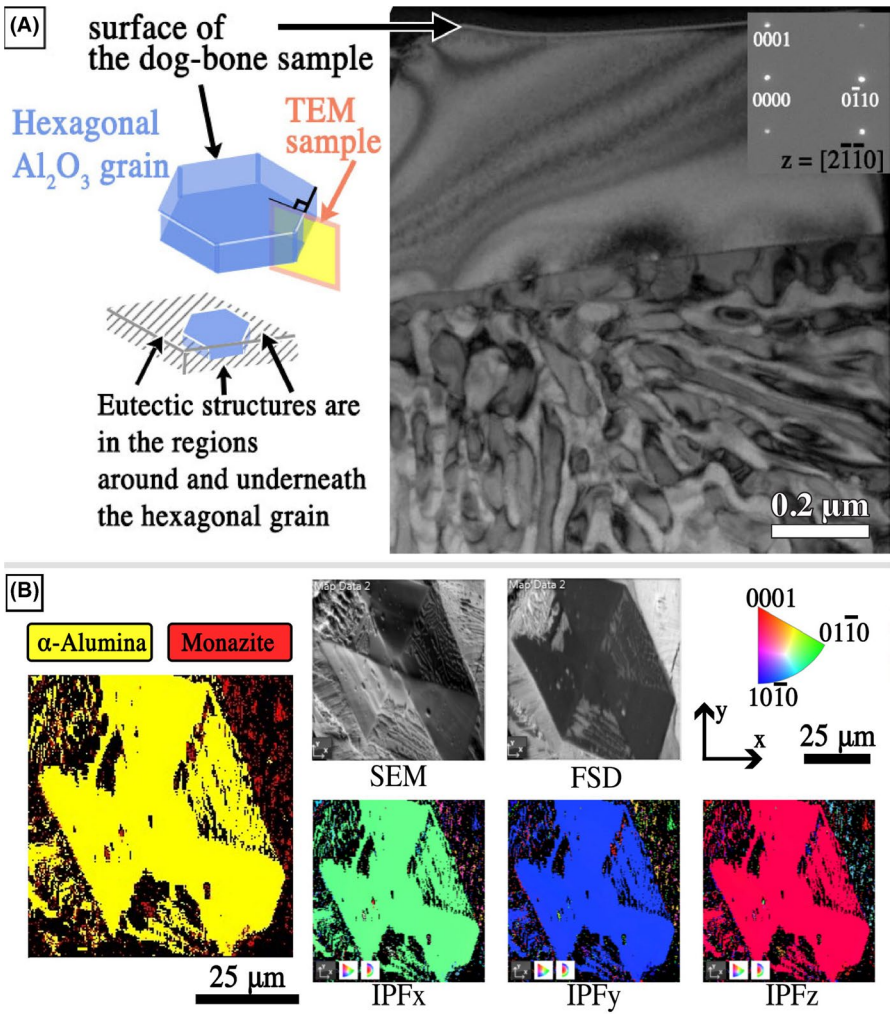

FIGURE 11 The orientation of the hexagonal alumina grains (A) image and diffraction pattern of a cross-section showing the (0 0 0 1) surface orientation of the hexagonal Al_2O_3 grain and eutectic microstructure underneath and (B) EBSD patterns showing that the large hexagonal Al_2O_3 grains on the surface are primarily one orientation (FSD images are obtained by a forward-scattered electron detector that collect backscattered electrons; graphs labeled IPFxyz show the crystalline orientation in the x, y, and z direction respectively, by coloring the maps with inverse pole figure color schemes) [Color figure can be viewed at wileyonlinelibrary.com]

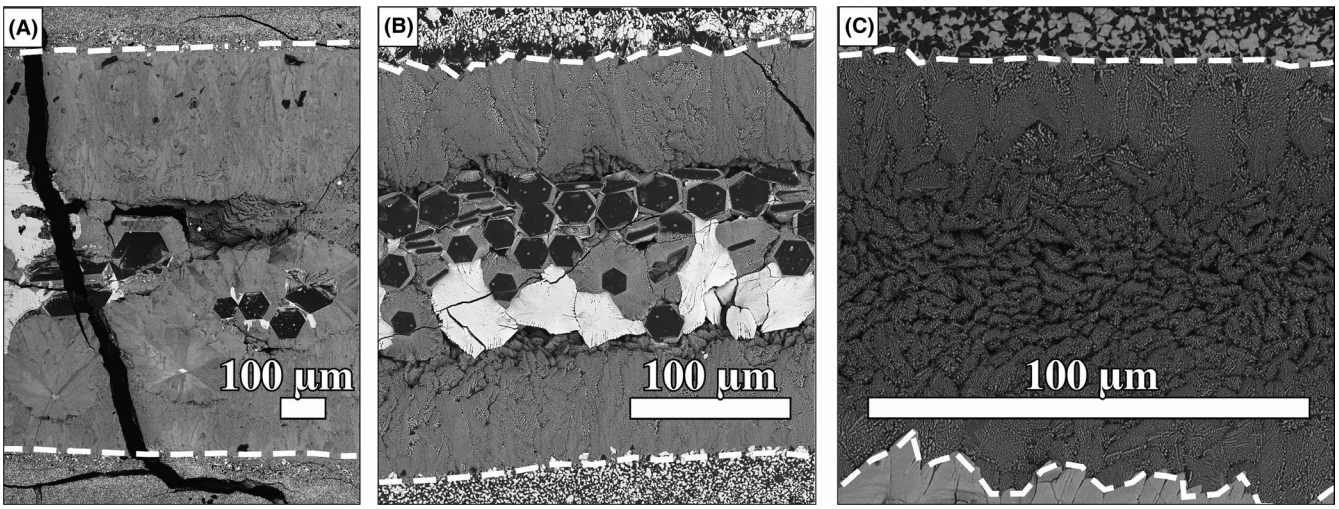

FIGURE 12 BSE images of flash sintered 50-50% Al_2O_3-$LaPO_4$ sample surfaces with different current limits of (A) **25** mA/mm^2 (1100 V/cm 8 s), (B) **5** mA/mm^2 (1050 V/cm 8 s), and (C) **2** mA/mm^2 (1136 V/cm 10 s); the higher the current, the wider the channeled region (note that the scale bar is different for each image). The electrical field is in the horizontal direction of the photo.

the composition changed to 25-75% Al_2O_3-$LaPO_4$ and 75-25% Al_2O_3-$LaPO_4$, the onset voltage of flash is noticeably lower (up to 100 V), as shown in Table 1. At first glance, it is unclear where the voltage difference comes from. Without the existence of 8YSZ that facilitates a conductive pathway,[41] low ionic and electrical conductivity of Al_2O_3 or

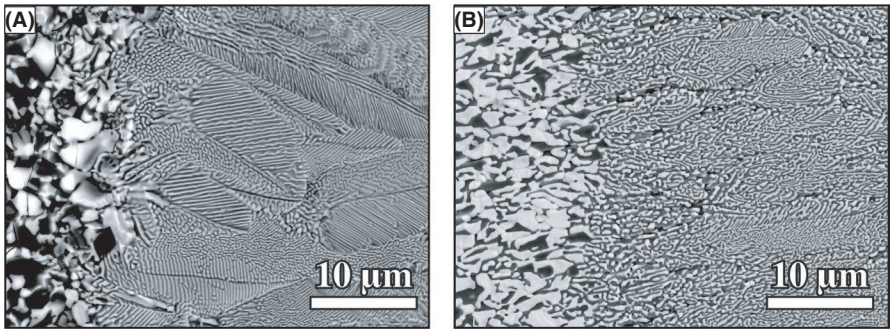

FIGURE 13 BSE images of eutectic structures on the surfaces of 50-50% Al_2O_3-$LaPO_4$ samples that depend on the current density showing (A) more regular eutectic-like structure that is produced under high current limit 25 mA/mm^2 (950 V/cm, 18 s), and (B) more irregular eutectic-like structure under low current limit 5 mA/mm^2 (1100 V/cm, 10 s). These images are from the edge of the channeled region, next to the polycrystalline structure, randomly oriented alumina and monazite grains are seen on the left of each image

$LaPO_4$ single phases inhibit the current flow. One reasonable hypothesis is that the bi-material interface in the green body can facilitate flash sintering, which could potentially be attributed to the highly defective structure of such bi-material grain boundaries. Alternatively, it could be doping by cations that would increase conductivity, but this needs to be further studied to be confirmed.[32] Other composites have been shown to flash easier than the single-phase materials without the presence and assistance of 8YSZ.[13] The 50%-50% Al_2O_3–$LaPO_4$ composites would have the maximum number of bi-material interfaces compared to other vol% compositions for the same particle sizes.

4.2 | What is the sample temperature during flash and how is it related to current?

It has been well known that the electrical field can elevate the sample temperature to be higher than the furnace temperature.[42] According to the black body radiation model (BBR)[7,43] which assumes the sample is a black body, the elevation in sample temperature (ΔT) can be calculated based on the furnace temperature (T_0 in K), the input power density (W_v equals voltage density times current density, in units of W m^{-3}), the volume of the sample (V with the value of 225 mm^3), material emissivity (e_m), the surface area of the sample (A with the value of 380 mm^2 including all surface area), and a universal physical constant (σ with the value of 5.67×10^{-8} W m^{-2} K^{-4}). The normal total emissivity of 8YSZ is estimated to be 0.4 around 1800°C[44] (0.9 at room temperature) [45] and Al_2O_3 is 0.3-0.5 at 1470°C.[46]

$$\frac{T}{T_0} = \left[1 + \frac{W_v}{e_m \sigma {T_0}^4}\left(\frac{V}{A}\right)\right]^{1/4} \quad (1)$$

However, experimental data is lacking on composites and there is no known emissivity data for $LaPO_4$, hence the calculations used emissivity values of unity[7] and 0.4 to estimate the range of possible sample temperatures (see Table 1 under column "BBR $T_{estimated}$"). The usage of unity can underestimate the sample temperature[7] by hundreds of degrees, having eliminated the emissivity in the denominator in Equation 1, giving the lower bound of the possible sample temperature range; the upper bound of the temperature range is given by using 0.4 as the emissivity value, which likely results in an overestimation of the sample temperature because of heat loss from the sample and the unknown emissivity value of $LaPO_4$.

The melting temperature of Al_2O_3 is 2030°C and 2070°C for monazite.[47,48] If a eutectic exists, the eutectic temperature would be even lower. With some of the estimated temperatures as high as 2190°C, and considering the underestimation of the lower bound calculation, it is reasonable for the actual sample temperature during flash to be higher than the melting point and the energy would be sufficient to cause melting. Also, the variable localized current observed on the surface (Figure 3) would cause inhomogeneous temperatures that are higher than the predicted average temperature. Furthermore, the area of the channeled region on the cross-section in Figure 9, corresponding to the high current pathway, is significantly smaller than the gauge section – concentrating the heating further. It is also possible that a small amount of eutectic liquid can form at the interfaces which would enhance sintering as well as the local current.[49,50]

4.3 | How do current, temperature, and channeling affect the microstructure?

The low thermal conductivity of $LaPO_4$[35] can preclude effective heat transfer; although Al_2O_3 has higher thermal conductivity than 8YSZ in the monazite materials, the lower electrical conductivity in alumina contributes to a current flow that is less uniform. This created a molten

and resolidified zone with distinct boundaries where the temperatures are higher. The abrupt boundaries can also be attributed to the temperature profile created by intense joule heating caused by the power spike. Heat can dissipate through conduction and convection due to the temperature difference within the sample and the elevation of sample temperature above the furnace temperature, but the abrupt boundaries of the channeled region are indications that the intense heat has not dissipated, and melting and rapid solidification only occurs within the boundaries. Research on flash sintering of Al_2O_3-$Y_3Al_5O_{12}$ (YAG) has shown the formation of similar eutectic microstructures but the paper postulates that melting does not occur.[26] The Al_2O_3/YAG system is similar to Al_2O_3–$LaPO_4$ in that YAG also has low conductivity[51] and is also observed to be difficult to flash sinter (1350°C, 900 V/cm).[26]

The estimated temperature correlated with the power input can qualitatively explain the trend of the channeled region widths. When the current density limit or the voltage density of the flash increases, the power increases – and as shown by Equation 1, the highest temperature in the channeled region caused by the power spike also increases, leading to more material melting.

It was observed that higher current limit also promotes abnormal grain growth and leads to the large single crystals forming in the channeled region (Figure 10). As the flash region temperature increases with the current, more time is needed to cool down whereby the crystals can grow quickly in what is possibly a eutectic liquid. There can also be a change in the nucleation rate that comes with the temperature change. At higher temperatures, one possible scenario is that the nucleation rate decreases while the growth rate increases, leading to fewer but larger crystals in the eutectic matrix.

Cracking has been observed in many samples produced in this study. During the experiment, the power supply and furnace were shut down right after the flash hold. This may induce thermal shock of the samples. It should be noted that when the samples were annealed at 1450°C after completion of the 11 seconds flash hold instead of instantaneously cooling, crack formation was minimized.

4.4 | How do surface and interfacial energy affect the resultant microstructure?

Al_2O_3 and $LaPO_4$ are highly immiscible. The XRD peaks of each phase do not shift before and after flash sintering, indicating no significant solid solubility. These materials do not react to form any new phases up to 1600°C, as proven by Marshall et al,[52] and the present study shows that to be true up to melting, which is useful information for the high-temperature applications of the material system.

The tendency to minimize the interfacial area between Al_2O_3 and $LaPO_4$ can be observed by the spherodized monazite in the lamellae (Figure 7A) and on the surface of alumina crystals, consistent with the predicted high interfacial energy between the two phases.[27] The sides of the faceted alumina crystals are also low-index planes that have high symmetry and low surface energy.[53] The facets may be evidence of crystallization from a melt that exists when alumina starts to nucleate and grow. The apparent 3-fold rotational symmetry shown by the monazite arrangement on the surface of the alumina grains (Figure 10) is linked to the crystallographic structure and inherent symmetry of the α-alumina crystal (with space group #167, $R\bar{3}c$) and corresponds directly to the primary 3-fold roto-inversion axis aligned along the c-axis of sapphire.[54] This observation portends that there is growth direction dependent variations, such that the prismatic planes are not all equivalent and alternate according to the 3-fold roto-inversion symmetry. Future work is in progress to explore details of the interfacial energy considerations in this material system.

4.5 | What factors may control the microstructure evolution of the eutectic?

The mechanism of forming regular and irregular eutectics in this material system is unknown. Even though directional cooling is evident in the orientation of the colonies growing perpendicular to the polycrystalline region in Figure 9, it is highly likely that more than one mechanism is at play due to the complicated thermal profiles of the molten and resolidified region.

The other possible cause of the "irregular eutectic" microstructure is that the phase transition has entered the region for spinodal transformations. The microstructures in Figure 7B are reminiscent of spinodal decomposition, however, it would be necessary to capture the initial phase segregation in the liquid to differentiate between nucleation and growth and processes and spinoidal decomposition.

According to past literature, the discontinuity and structural faults in the regular lamellar structure can be caused by several different reasons, including liquid/solid interface shape instability, lattice strain, or sudden change in the growth conditions, etc.[38,39] Lamellar eutectic-like structures usually represent fast coupled growth of the crystallization front, the rate of which is a function of the undercooling in the composite system.[55] At the same time, it is known that drastically increasing the amount of undercooling can change the type of eutectic structure formed.[56] In theory, the irregular eutectic structures can be an indication of different growth velocities.

Although it is not clear which mechanism dominates, it is obvious that higher power applied from high currents

promotes regular lamellar eutectic microstructures. These eutectic microstructures, with a characteristic lamellae thickness on a scale of 100 nm, have the potential for interesting mechanical properties promoting crack arrest.[57,58] Current work is on-going to evaluate the mechanical properties of such microstructures.

5 | CONCLUSION

- As expected, composites of monazite and 8YSZ can be easily flash sintered due to the enabling presence of 8YSZ which allows uniform heating of the composite. Although higher amounts of 8YSZ lowered the furnace flash temperature, 25 vol% 8YSZ was sufficient to create a uniform microstructure.
- Single phase Al_2O_3 and $LaPO_4$ did not flash under the maximum temperature and voltage used here, but the binary composites did, indicating that heterointerfaces may play a significant role in flash sintering as pathways for high current density.
- Regions in the Al_2O_3–$LaPO_4$ sample where the temperature was close to the furnace temperature produced microstructures similar to conventionally sintered polycrystalline samples; channeled regions with the higher current that reached the highest temperature show nucleation and growth of large crystals of faceted alumina and non-faceted monazite; with lower current and lower temperature, large regions of relatively uniform eutectic microstructures can be formed in the channeled regions, presumably nucleated from the liquid phase.
- More regular regions of the eutectic tend to form when the current density is higher while irregular eutectic forms when it is lower.
- There is immiscibility of alumina and monazite even at elevated temperatures with a high interfacial energy between the two phases, as demonstrated by the eutectic microstructure.

Further work is in progress to determine the high-temperature phase diagram of alumina and monazite and evaluate the mechanical properties of the regular and irregular eutectic structures as well as the single crystals that form. Flash sintering may have potential in making eutectic structures without requiring ultra-high temperature melting in non-reactive crucibles.

ACKNOWLEDGEMENTS

This material is based upon work supported by the National Science Foundation under Grant No. CMMI 1662791. Any opinions, findings, and conclusions or recommendations expressed in this material are those of the authors and do not necessarily reflect the views of the National Science Foundation. XRD, SEM, EBSD, FIB, and TEM work were performed at the UC Irvine Materials Research Institute (IMRI). Part of the FIB work was performed using instrumentation funded in part by the National Science Foundation Center for Chemistry at the Space-Time Limit (CHE-082913). The authors would like to thank Rishi Raj and his group members in helping us build our flash sintering setup based on their prototype, and to thank David Kok for coordinating the build.

AUTHOR CONTRIBUTIONS

Yingjie Yang contributed to experimental work and draft of the paper; Daniel Mumm contributed to writing advice and data analysis advice; Martha Mecartney was the project advisor and contributed to experimental funding and support, and writing advice.

ORCID

Yingjie Yang https://orcid.org/0000-0002-1898-8171

REFERENCES

1. Cologna M, Rashkova B, Raj R. Flash sintering of nanograin zirconia in <5 s at 850°C. J Am Ceram Soc. 2010;93(11):3556–9.
2. Charalambous H, Jha SK, Lay RT, Cabales A, Okasinski J, Tsakalakos T. Investigation of temperature approximation methods during flash sintering of ZnO. Ceram Int. 2018;44(6):6162–9.
3. Todd RI, Zapata-Solvas E, Bonilla RS, Sneddon T, Wilshaw PR. Electrical characteristics of flash sintering: thermal runaway of Joule heating. J Eur Ceram Soc. 2015;35(6):1865–77.
4. Yu M, Grasso S, Mckinnon R, Saunders T, Reece MJ. Review of flash sintering: materials, mechanisms and modelling. Adv Appl Ceram. 2017;116(1):24–60.
5. Agrafiotis C, Tsoutsos T. Energy saving technologies in the European ceramic sector: a systematic review. Appl Therm Eng. 2001;21(12):1231–49.
6. Tikul N, Srichandr P. Assessing the environmental impact of ceramic tile production in Thailand. J Ceram Soc Japan. 2010;118(1382):887–94.
7. Raj R. Joule heating during flash-sintering. J Eur Ceram Soc. 2012;32(10):2293–301.
8. Raj R, Cologna M, Prette ALG, Sglavo VM, Luiz A, Prette G, et al. Methods of flash sintering. United States patent US008940220. 2015.
9. Zhang Y, Nie J, Chan JM, Luo J. Probing the densification mechanisms during flash sintering of ZnO. Acta Mater. 2017;125:465–75.
10. M'Peko J-C, Francis JSC, Raj R. Field-assisted sintering of undoped $BaTiO_3$: microstructure evolution and dielectric permittivity. J Eur Ceram Soc. 2014;34(15):3655–60.
11. Dychtoń K, Drajewicz M, Pytel M, Rokicki P, Nowotnik A. Yttria-stabilized zirconia–alumina composite sintering temperature effect on thermal diffusivity. J Therm Anal Calorim. 2016;126(1):1–7.
12. Kok D, Yadav D, Sortino E, McCormack SJ, Tseng K-P, Kriven WM, et al. α-Alumina and spinel react into single-phase high-alumina spinel in <3 seconds during flash sintering. J Am Ceram Soc. 2018;102(2):644–53.
13. Kok D, Jha SK, Raj R, Mecartney ML. Flash sintering of a three-phase alumina, spinel, and yttria-stabilized zirconia composite. J Am Ceram Soc. 2017;100(7):3262–8.

14. Bichaud E, Chaix JM, Carry C, Kleitz M, Steil MC. Flash sintering incubation in Al_2O_3/TZP composites. J Eur Ceram Soc. 2015;35(9):2587–92.
15. Yoon B, Avila V, Kathiria R, Jesus LM. Effects of powder dispersion on reactive flash sintering of 8 mol% yttria-stabilized zirconia and $MgAl_2O_4$ composites. Scr Mater. 2020;189117–21.
16. Biesuz M, Sglavo VM. Flash sintering of alumina: effect of different operating conditions on densification. J Eur Ceram Soc. 2016;36(10):2535–42.
17. Biesuz M, Sglavo VM. Liquid phase flash sintering in magnesia silicate glass-containing alumina. J Eur Ceram Soc. 2017;37(2):705–13.
18. Cologna M, Francis JSC, Raj R. Field assisted and flash sintering of alumina and its relationship to conductivity and MgO-doping. J Eur Ceram Soc. 2011;31(15):2827–37.
19. Liu D, Gao Y, Liu J, Liu F, Li K, Su H, et al. Preparation of Al_2O_3–$Y_3Al_5O_{12}$–ZrO_2 eutectic ceramic by flash sintering. Scr Mater. 2016;114108–11.
20. Biesuz M, Luchi P, Quaranta A, Sglavo VM. Theoretical and phenomenological analogies between flash sintering and dielectric breakdown in α-alumina. J Appl Phys. 2016;120(14):145107.
21. Yoshida H, Biswas P, Johnson R, Mohan MK. Flash-sintering of magnesium aluminate spinel ($MgAl_2O_4$) ceramics. J Am Ceram Soc. 2017;100(2):554–62.
22. Naik K, Jha SK, Raj R. Correlations between conductivity, electroluminescence and flash sintering. Scr Mater. 2016;1181–4.
23. Liu D, Gao Y, Liu J, Li K, Liu F, Wang Y, et al. SiC whisker reinforced ZrO_2 composites prepared by flash-sintering. J Eur Ceram Soc. 2016;36(8):2051–5.
24. Gaur A, Sglavo VM. Flash sintering of (La, Sr)(Co, Fe)O_3-Gd-Doped CeO_2 composite. J Am Ceram Soc. 2015;98(6):1747–52.
25. Francis JSC, Cologna M, Montinaro D, Raj R. Flash sintering of anode-electrolyte multilayers for SOFC applications. J Am Ceram Soc. 2013;96(5):1352–4.
26. Liu J, Xu X, Liu D, Chen L, Zhao K, An L. Ultrafast formation of Al_2O_3 –$Y_3Al_5O_{12}$ eutectic ceramic by flash sintering. J Am Ceram Soc. 2020;103(8):4051–6.
27. Marshall DB, Morgan PED, Housley RM. Debonding in multilayered composites of zirconia and $LaPO_4$. J Am Ceram Soc. 2005;80(7):1677–83.
28. Davis JB, Marshall DB, Morgan PED. Oxide composites of Al_2O_3 and $LaPO_4$. J Eur Ceram Soc. 1999;19(13–14):2421–6.
29. Morgan PED, Marshall DB. Ceramic composites of monazite and alumina. J Am Ceram Soc. 1995;78(6):1553–63.
30. Zhang C, Fei J, Guo L, Yu J, Zhang B, Yan Z, et al. Thermal cycling and hot corrosion behavior of a novel $LaPO_4$/YSZ double-ceramic-layer thermal barrier coating. Ceram Int. 2018;44(8):8818–26.
31. Ren X, Guo S, Zhao M, Pan W. Thermal conductivity and mechanical properties of YSZ/$LaPO_4$ composites. J Mater Sci. 2014;49(5):2243–51.
32. Raj R, Cologna M, Francis JSC. Influence of externally imposed and internally generated electrical fields on grain growth, diffusional creep, sintering and related phenomena in ceramics. J Am Ceram Soc. 2011;94(7):1941–65.
33. Marshall D. Ceramics for future power generation technology: fiber reinforced oxide composites. Curr Opin Solid State Mater Sci. 2001;5(4):283–9.
34. Sudre OH, Marshall DB, Morgan PED. Monazite-based thermal barrier coatings. Washington, DC, United States patent US6863999. 2005.
35. Min W, Miyahara D, Yokoi K, Yamaguchi T, Daimon K, Hikichi Y, et al. Thermal and mechanical properties of sintered $LaPO_4$-Al_2O_3 composites. Mater Res Bull. 2001;36(5–6):939–45.
36. Min W, Daimon K, Matsubara T, Hikichi Y. Thermal and mechanical properties of sintered machinable $LaPO_4$–ZrO_2 composites. Mater Res Bull. 2002;37(6):1107–15.
37. Men D, Mecartney ML. Superplasticity and machinability in a four-phase ceramic. Mater Res Bull. 2012;47(8):1925–31.
38. Croker MN, Baragar D, Smith RW. Anomalous eutectic growth. J Cryst Growth. 1975;30(2):198–212.
39. Stubican VS, Bradt RC. Eutectic solidification in ceramic systems. Annu Rev Mater Sci. 1981;11(1):267–97.
40. Dong Y, Chen I-W. Onset criterion for flash sintering. J Am Ceram Soc. 2015;98(12):3624–7.
41. Zapata-Solvas E, Bonilla S, Wilshaw PR, Todd RI. Preliminary investigation of flash sintering of SiC. J Eur Ceram Soc. 2013;33(13–14):2811–6.
42. Francis JSC, Raj R. Influence of the field and the current limit on flash sintering at isothermal furnace temperatures. J Am Ceram Soc. 2013;96(9):2754–8.
43. Jha SK, Lebrun JM, Raj R. Phase transformation in the alumina–titania system during flash sintering experiments. J Eur Ceram Soc. 2016;36(3):733–9.
44. Mosley FH. Experimental determination of emissivity and resistivity of yttria stabilized zirconia at high temperatures. Knoxville: The University of Tennessee; 2008.
45. Tanaka H, Sawai S, Morimoto K, Hisano K. Measurement of spectral emissivity and thermal conductivity of zirconia by thermal radiation calorimetry. J Therm Anal Calorim. 2001;64(3):867–72.
46. Touloukian YS, Dewitt DP. Thermophysical properties of matter - The TPRC Data Series. Volume 8. Thermal radiative properties - nonmetallic solids. 1972.
47. Geller RF, Yavorsky PJ. Melting point of alpha-alumina. J Res Natl Bur Stand. 1945;34(4):395.
48. Hikichi Y, Nomura T. Melting temperatures of monazite and xenotime. J Am Ceram Soc. 1987;70(10):C-252–3.
49. Chaim R. Particle surface softening as universal behaviour during flash sintering of oxide nano-powders. Materials (Basel). 2017;10(2):179.
50. Chaim R, Amouyal Y. Liquid-film assisted mechanism of reactive fash sintering in oxide systems. Materials (Basel). 2019;12(9):1494.
51. Wang J, Xu F, Wheatley RJ, Neate N, Hou X. Yb^{3+} doping effects on thermal conductivity and thermal expansion of yttrium aluminium garnet. Ceram Int. 2016;42(12):14228–35.
52. Marshall DB, Morgan PED, Housley RM, Cheung JT. High-temperature stability of the Al_2O_3-$LaPO_4$ system. J Am Ceram Soc. 2005;81(4):951–6.
53. Morrissey KJ, Carter CB. Faceted grain boundaries in Al_2O_3. J Am Ceram Soc. 2006;67(4):292–301.
54. Arnold H, Aroyo MI, Bertaut EF, Burzlaff H, Chapuis G. Space-group symmetry. In: Hahn T, Aroyo MI, editors. International Tables for Crystallography. Chester, England: International Union of Crystallography; p.
55. Wang Z-G, Ouyang J-H, Ma Y-H, Wang Y-J, Xie L-Y, Henniche A, et al. Enhanced nucleation undercooling and surface self-nanocrystallization of Al_2O_3-ZrO_2(Y_2O_3) eutectic ceramics. J Eur Ceram Soc. 2019;39(4):1707–11.
56. Han XJ, Wang N, Wei B. Rapid eutectic growth under containerless condition. Appl Phys Lett. 2002;81(4):778–80.

57. Peña JI, Larsson M, Merino RI, de Francisco I, Orera VM, LLorca J, et al. Processing, microstructure and mechanical properties of directionally-solidified Al_2O_3–$Y_3Al_5O_{12}$–ZrO_2 ternary eutectics. J Eur Ceram Soc. 2006;26(15):3113–21.
58. Kim WY, Tanaka H, Kasama A, Hanada S. Microstructure and room temperature fracture toughness of Nb_{ss}/Nb_5Si_3 in situ composites. Intermetallics. 2001;9(9):827–34.

How to cite this article: Yang Y, Mumm DR, Mecartney ML. Flash sintering produces eutectic microstructures in Al_2O_3–$LaPO_4$ versus conventional microstructures in 8YSZ–$LaPO_4$. *J Am Ceram Soc*. 2021;104:3895–3909. https://doi.org/10.1111/jace.17786